DOI: 10.1002/fuce.201900245

Fuel Cells

ORIGINAL RESEARCH PAPER

Long-Term Behavior of a Solid Oxide Electrolyzer (SOEC) Stack▲

M. Lang[1]*, S. Raab[1], M. S. Lemcke[1], C. Bohn[1], M. Pysik[1]

[1] German Aerospace Center (DLR), Pfaffenwaldring 38–40, 70569 Stuttgart, Germany

Received June 15, 2020; accepted September 08, 2020; published online ■■■

Abstract

The successful market introduction of the solid oxide fuel/electrolysis cell technology for power-to-gas applications requires the reduction of the degradation rates and the better understanding of the degradation mechanisms of the stacks. Therefore, the paper reports and compares the long-term behavior of a solid oxide cell stack in electrolysis and reversible fuel cell/electrolysis operation. The 30-cell stack with electrolyte supported cells was supplied by Sunfire GmbH (Dresden/Germany) in the German funded RSOC Project. The stack was operated for 3,370 h in electrolysis and afterwards for 2,500 h in reversible fuel cell/electrolysis mode, each at 70% gas conversion. In the beginning of the test, the stack showed high gas tightness, good performances and high efficiencies in both SOEC and SOFC operations. During 3,370 h of SOEC operation a low degradation of +0.5%/1,000 h was measured. During 2,500 h of reversible fuel cell/electrolysis cycling, the gas tightness of the stack slightly decreased, which led to a temperature increase, and higher degradation rates were observed. The increase of the ohmic resistance contributed mostly to the degradation. Optimized operating conditions for reversible cycling and increasing the purity of the supplied water are foreseen in order to minimize stack degradation in reversible operation.

Keywords: Degradation, Electrochemical Impedance Spectroscopy, Electrochemistry, Fuel Cell, High Temperature Electrolysis, Hydrogen, Reversible Operation, Solid Oxide Electrolysis, Solid Oxide Electrolysis Cell, Solid Oxide Fuel Cell, Stack

1 Introduction

The successful market introduction and public acceptance of the high temperature solid oxide cells (SOC) technology require high performance, long-term stability and low costs of the corresponding stacks. This technology has several advantages compared to low temperature cells. Firstly, the cells can be operated reversely in electrolysis (SOEC) and fuel cell (SOFC) mode, which predestines this technology for power-to-gas applications. Secondly, SOCs can be applied to the H_2/H_2O and the CO/CO_2 redox systems, thus generating electrical energy from carbon containing fuels (e.g., natural gas) in fuel cell mode and producing so-called "syngas" in electrolysis mode. Thirdly, at the high temperatures of 700 °C–850 °C, the required entropic heat demand for the endothermic decomposition of steam is lower compared to liquid water [1], which results in low power consumption [2]. Although the degradation rates of solid oxide electrolysis (SOE) cells and stacks have been steadily decreased in recent years [3], the understanding of degradation and degradation mechanisms remain the most important and challenging issues [4]. Only few documents can be found in literature, which address the stack degradation in electrolysis mode for more than 500 h of operation [5–18]. The knowledge gap for SOEC stack degradation in reversible SOFC/SOEC operation mode is even wider. Few relevant degradation results can be found in [19–24]. Therefore, this paper reports and compares the long-term behavior of a SOC stack in SOFC and reversible SOFC/SOEC operation. The results have been presented 2019 at the 16. International Conference on Solid Oxide Fuel Cells (SOFC 16) [25].

1.1 SOFC/SOEC Technology

Figure 1 shows an example of a SOC with the corresponding electrochemical reactions during water electrolysis. The shown cell is mechanically supported by a thick solid oxygen

▲ *Invited paper related to the Topical Issue on "High-Temperature Electrolysis using Solid Oxide Electrolyzer Cell (HT-SOEC)".*

[*] *Corresponding author, michael.lang@dlr.de*

ion conductive yttrium stabilized zirconium dioxide (YSZ) electrolyte (electrolyte supported cell, ESC). Another option is to support the cell by a thick porous fuel electrode substrate (anode supported cell, ASC) or by a porous metal substrate (metal supported cell, MSC). The negative fuel electrode usually consists of a porous ceramic-metal (cermet) compound, made either of nickel and gadolinium doped cerium dioxide (GDC) or of nickel and YSZ. The positive porous air electrode normally consists of lanthanum-strontium-cobalt ferrite (LSCF) mixed with either GDC or YSZ. Very often a current collector layer is applied on top of the air electrode.

Both reactants H_2O and/or CO_2 can be converted, however the present paper focuses on the H_2/H_2O redox system. By supplying electrons from a voltage source to the fuel electrode, steam is reduced to H_2 by the following reaction (Eq. (1)). The resulting O^{2-}-ions migrate through the solid ceramic electrolyte and are oxidized to oxygen molecules at the air electrode (Eq. (2)).

$$H_2O + 2e^- \rightarrow H_2 + O^{2-} \tag{1}$$

$$O^{2-} \rightarrow \frac{1}{2}O_2 + 2e^- \tag{2}$$

The overall endothermic reaction for steam electrolysis is:

$$H_2O \rightarrow H_2 + \frac{1}{2}O_2 \tag{3}$$

In the following section the important formulas of the SOC technology are given. An entire survey and description of the nomenclature and formulary can be found in the documents of the European funded SOCTESQA ("Solid Oxide Cell and Stack Testing, Safety and Quality Assurance") project [26] and of the International Electrotechnical Commission [27, 28].

The measurable open circuit voltage *(OCV)* can be calculated by subtracting the irreversible loss η_0 [26] from the theoretical thermodynamic reversible cell voltage $V_{rev}(T)$, which itself is described by the Nernst equation:

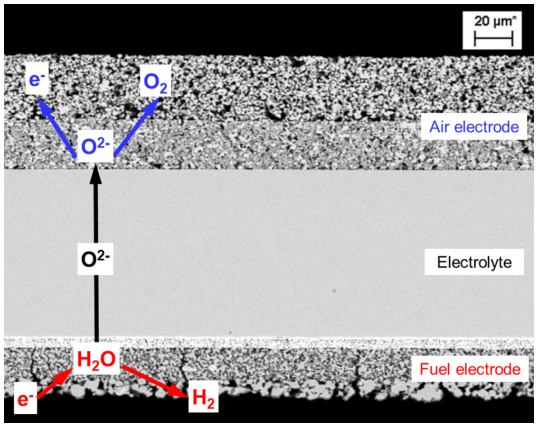

Fig. 1 Example of a SOC with the corresponding electrochemical reactions for water electrolysis.

$$OCV = \left(V_{rev}^0(T) + \frac{RT}{zF} \cdot \ln \frac{p_{O_2}^{1/2} \cdot p_{H_2}}{p_{H_2O}} \right) - \eta_0 \tag{4}$$

where V_{rev}^0 is the reversible cell voltage for partial pressure of 1, R is the gas constant, z is the number of electrons (2), F is Farady's constant, p is partial pressure, and η_0 is the irreversible loss due to intermediate reaction species and the resulting mixed potential at the electrodes.

The electrolysis voltage $V(I)$ under operation at an electrical current I is the sum of the OCV and the resulting overvoltages ΔV_{total}, which are generated by the resistances of the cell or the stack repeat unit. These can be classified in polarization (R_{Pol}), ohmic (R_{Ohm}) and gas diffusion or gas concentration resistances (R_{GC}):

$$V(I) = OCV + \int_I (R_{Pol}(I) + R_{Ohm}(I) + R_{GC}(I))dI \tag{5}$$

The overvoltage losses generate dissipative heat within the cell or stack repeat unit, which increases with increasing current density. Thermal equilibrium is reached when the dissipative overvoltage heat generation equals the required entropic heat $T \cdot \Delta rS\ (T)$ for water splitting. The resulting thermo-neutral voltage V_{tn} can be calculated from the molar enthalpy of reaction $\Delta rH\ (T)$ according to:

$$V_{tn}(T,p) = \frac{\Delta r\ H(T,p)}{2F} \tag{6}$$

At 820 °C a thermo-neutral voltage of 1.29 V can be calculated, which is based on the standard molar enthalpy of reaction ΔrH^0 (750 °C) for steam electrolysis of about 249 kJ mol^{-1} [29]. In the so-called "endothermal mode" the cell or RU is operated at voltages below the thermo-neutral voltage. In this case heat input from an external source is required in order to maintain a constant temperature. In the "exothermal mode" at voltages higher than V_{tn} the situation is vice-versa and excessive resistivity heat is supplied by the cell or RU.

The reactant gas utilization U_{gas} is the ratio of current I to the theoretical maximum current I_{theory}. U_{gas} is often called steam conversion (SC) in SOEC and fuel utilization (FU) in SOFC.

$$U_{gas} = I/I_{theory} = I/\left(\frac{F}{N} \cdot \sum_{i=1}^{n} z_i \cdot \frac{f_{i,\,in}}{V_{i,mol} \cdot 60s} \right) \tag{7}$$

where N is number of repeat units, and $f_{i,in}$ (slpm) and $V_{i,mol}$ are the inlet gas flow rate and molar volume of reactant component i.

The electrical efficiency η_{el} of an SOEC stack is the ratio of produced fuel gas power to the consumed electrolysis power P_{el}. For SOFC operation this is *vice versa*.

$$\eta_{el,LHV} = \frac{\sum_{i=1}^{n} LHV_i \cdot \frac{f_{i,out}}{V_{i,m} \times 60\ \mathrm{s}}}{P_{el}} \tag{8}$$

where LHV_i and $f_{i,out}$ are the lower heating value and volume flow of produced fuel gase component i.

Please note: Eq. (8) describes the electrical efficiency of an SOC stack, which differs from the efficiency of an SOC system. For a system the power consumption of the peripheral components, e.g., steam generator, heat exchangers and control unit, must also be considered in the calculation.

The absolute or relative degradation (ΔX, ΔX_{rel}) of a quantity X (e.g., p, V, ASR…) within a time interval t_2–t_1 are defined according to:

$$\frac{\Delta X}{\Delta t} = \frac{X(t_2) - X(t_1)}{t_2 - t_1} \tag{9}$$

and

$$\frac{\Delta X_{rel}}{\Delta t} = \frac{X(t_2) - X(t_1)}{X(t_1) \cdot (t_2 - t_1)} \cdot 100\% \tag{10}$$

2 Experimental

Figure 2 shows the experimental setup for testing of the SOC stack. The stack of this paper (type "MK225") consisted of 30 repeat units and was supplied by Sunfire GmbH (Dresden, Germany) in the frame of the RSOC (Reversible Solid Oxide Cell) project. For increasing the mechanical stability the stack was subdivided by intermediate plates after every 10 RUs. A special feature of the parallel co-flow stack design is the open air electrode. Electrolyte supported cells (similar to Figure 1) with an active area of 128 cm^2 were used in the stack. The cells have been originally developed for SOFC application and were modified for electrolysis operation. The cell is mechanically supported by an 80 µm thick dense YSZ electrolyte (3YSZ). A porous GDC barrier layer between electrolyte substrate and air electrode prevents inter-diffusion at the interface. The negative fuel electrode consists of a porous cermet of Ni and GDC. The positive porous air electrode consists of LSCF mixed with GDC. The cells were sealed with glass sealings on stamped metal sheet bipolar plates made of the ferritic steel "Crofer22APU" from ThyssenKrupp AG [30].

The gas inlet parameters are flow rate, composition, temperature and pressure. The gas inlet and outlet temperatures were measured with thermocouples, which were located just below the stack. The stack temperatures were measured with four thermocouples integrated at different positions in the stack. This enables the analysis of temperature gradients inside the stack. The electrical current probes were connected to the top and bottom plates, while the voltage probes were attached at each repeat unit of the stack. The mechanical load on the stack was 1,200 N.

After the initial performance test, the stack was operated during 3,370 h in SOEC operation mode and afterwards cycled for 2,500 h in reversible SOFC/SOEC operation mode at a constant steam conversion/fuel utilization of 70%, respectively. In order to achieve a high reproducibility and repeatability, all tests were conducted according to the pre-normative standardized test procedures of the SOCTESQA project [26]. Moreover, the derived quantities, e.g., steam conversion, fuel utilization, electrical efficiency and degradation, were calculated according to the formulas described in Section 1.

Table 1 lists the operating conditions for the long-term tests. The duration of a complete SOFC/SOEC cycle was 24 h with 8 h of SOEC operation at 820 °C, 8 h of SOFC operation at 750 °C as well as two switching phases, each with 4 h duration, for changing the test operating conditions between both modes. For SOFC and SOEC fuel gas mixtures of 40% H_2 + 60% N_2 and 80% H_2O + 9% H_2 + 11% N_2 were used, respectively. The N_2 addition in SOEC mode had the function to stabilize the steam supply, thus to minimize voltage fluctuations. The given temperatures in this paper refer to the thermocouple in the middle of the stack (RU 15) at OCV. The maximum stack temperature limit given by the stack supplier was 860 °C. Therefore, for the cooling of the stack in SOFC operation a high air flow rate of 6.7 SLPM/RU was chosen. Moreover, during reversible operation, the electrical current density and the fuel gas flow rate had to be adjusted in order to remain below 860 °C and to maintain 70% gas utilization, respectively. The degradation of the ASR was calculated by dividing the voltage increase by the applied electrical current density. Moreover,

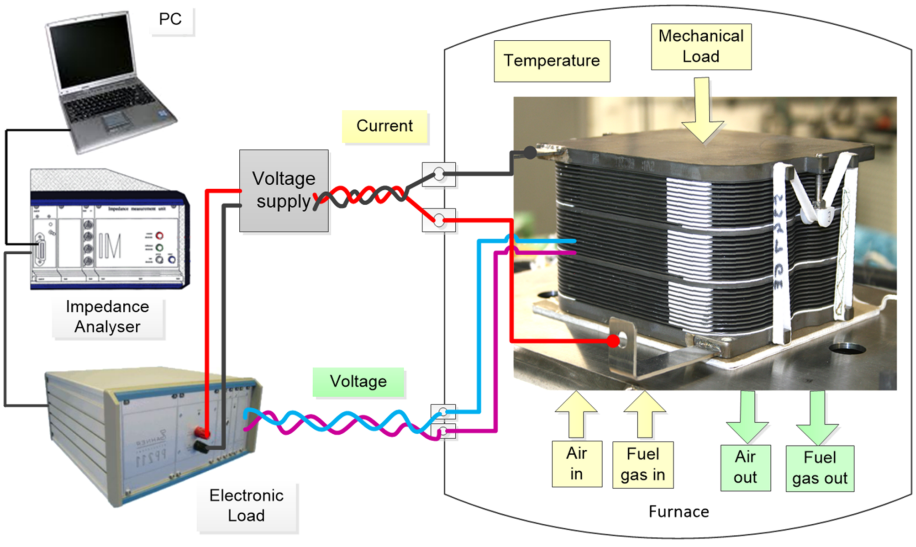

Fig. 2 Experimental setup for electrochemical characterization of the tested SOC stack.

Table 1 Operating conditions for SOEC and reversible SOFC/SOEC long-term tests.

Long-term operation	Electrolysis	Reversible electrolysis/fuel cell cycling	
Duration	3,370 h	2,500 h	
Mode	SOEC	SOEC	SOFC
Number / duration of cycles	/	92 × 12 h	97 × 12 h
Temperature	820 °C	820 °C	750 °C
Fuel gas composition	80% H_2O + 9% H_2 + 11% N_2	80% H_2O + 9% H_2 + 11% N_2	40% H_2 + 60% N_2
Fuel gas flow rate	0.833 SLPM/RU	0.609 SLPM/RU to 0.833 SLPM/RU	0.57 SLPM/RU
Air flow rate	1.0 SLPM/RU	1.0 SLPM/RU	6.7 SLPM/RU
Electrical current density	–520 mA cm^{-2}	–380 mA cm^{-2} to –520 mAcm^{-2}	180 mA cm^{-2}
Steam conversion / fuel utilization rate	70%	70%	70%

current-voltage (*J–V*) characteristics and electrochemical impedance spectra (EIS) were recorded regularly. For the *J–V*-characteristics the electrical current was increased and decreased very slowly with a rate of 7 mA s^{-1}, in order to reach quasi thermal equilibrium. A fast data sampling rate of 1 s was chosen in order to record possible voltage fluctuations.

The EIS spectra were measured with a "Zahner, Type IM6" impedance analyzer connected to an electronic load "EL 1000". For SOEC, a voltage supply was integrated in the current circuit (Figure 2). In order to minimize high frequency artifacts, the electrical current and voltage probes were twisted separately [31]. An AC amplitude of 15 mA cm^{-2} with a frequency range of 2 mHz to 500 kHz was applied to the stack. EIS spectra were recorded near OCV conditions, in order to analyze and qualify the degradation mechanisms without having electrical current induced temperature effects involved. These spectra do not focus on the quantification of the degradation values of the long-term operations, but on the analysis of the differences between SOEC and reversible SOFC/SOEC operation. A small direct current of -15 mA cm^{-2} for SOEC and +15 mA cm^{-2} for SOFC was applied in order to ensure that the stack remained in the required operating mode during the recording of the EIS spectra. The individual resistances, specifically the ohmic, electrode polarization and gas concentration resistance, of the RUs were determined from the Cole-Cole plots of the spectra. Please note, the corresponding impedance values refer to the low current density region (see Figure 3 below) and are much higher compared to the above calculated area specific resistance (ASR) values from the long-term operations at high electrical current load.

3 Results and Discussion

3.1 Initial SOC Stack Performance

Figure 3 shows the initial *J–V*-curve and the measured temperature in the middle of the SOC stack in electrolysis and fuel cell mode with increasing current density. The stack was operated at 820 °C with 40% H_2 + 60% N_2 in SOFC and with 80% H_2O + 9% H_2 + 11% N_2 in SOEC.

In SOFC the stack showed a high OCV of about 38 V, which corresponds to an average OCV of the RUs of 1.27 V. This value is in good agreement with the theoretical value of 1.31 V calculated with the Nernst equation based on a fuel gas composition of 40% H_2 + 60% N_2 and a gas purity of 99.99%. The difference between both values can be explained by small leakages at the compressive sealing between gas distribution plate and stack bottom plate. Hence, a high gas tightness of the stack is proven. A nonlinear progression of the *J–V*-curve with increasing current density can be observed. This behavior is typical for stacks with high gas tightness, which are operated with dry fuel gas in SOFC mode. EIS spectra measured with increasing current density up to 50 mA cm^{-2} (not shown here) have revealed a strong decrease of the gas concentration resistance at the fuel gas side, leading to the observed significant reduction of the ASR. The gas concentration resistance will be explained more detailed below in Section 3.5. At current densities higher than 50 mA cm^{-2} the *J–V*-curve proceeds

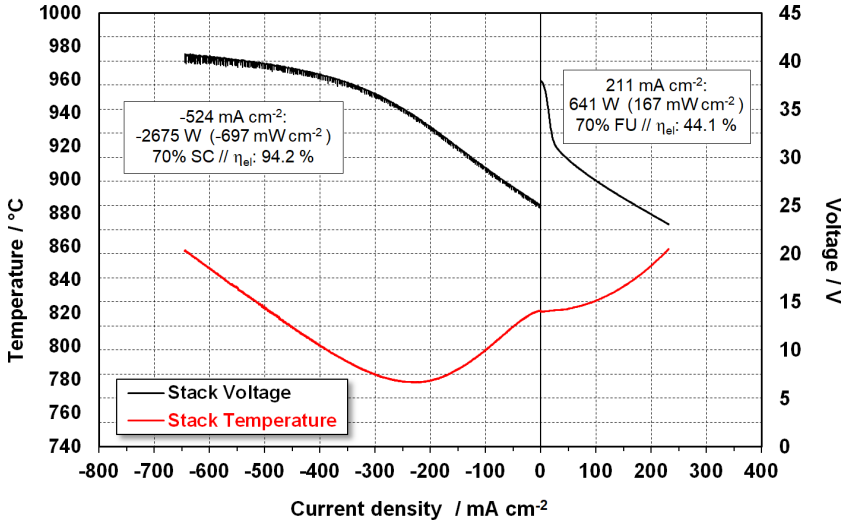

Fig. 3 Current density-voltage curve of 30-cell SOC stack at 820 °C with 80% H_2O + 9% H_2 + 11% N_2 in SOEC and with 40% H_2 + 60% N_2 in SOFC.

almost linearly. The EIS spectra measured up to 210 mA cm^{-1} have shown reducing ohmic and polarization resistances with increasing stack temperature and increasing gas concentration resistances, due to gas transport limitations in the porous structure of the fuel electrodes. The maximum stack temperature limit of 860 °C was already reached at a current density of ca. 240 mA cm^{-2} in SOFC mode. Hence, no significant diffusion limitation overvoltage can be observed in SOFC mode. In order to evaluate the performance of the stack in SOFC, the values at 70% fuel utilization were determined. 70% FU was reached at ca. 210 mA cm^{-2}, at a stack voltage of nearly 24 V and a stack temperature of ca. 850 °C. This results in a stack power of 640 W and a power density of ca. 170 mW cm^{-2} with an electrical efficiency of 44%. These values are in the same range or even higher compared to literature data [10, 24, 32]. Moreover, the performance of the 30 RUs of the stack was almost homogeneous. The ASR and voltage values of the RUs at 70% FU were in the range from 1.20 Ω cm^2 to 1.40 Ω cm^2 and 780 mV to 800 mV, respectively. The RUs located on the bottom plate (RU 1), on the intermediate plates (RU 11 and RU 21) and under the top plate (RU 30) of the stack (see Figure 2) reached slightly lower performances. EIS spectra of these RUs have shown higher ohmic resistances compared to the other RUs, which can be attributed to higher contact resistances. The observed temperature gradients over the height of the stack were low. The slightly higher temperatures in the middle of the stack did not significantly affect the performance of the corresponding RUs. Hence, the tested stack showed a good initial SOFC performance with acceptable homogeneity.

In SOEC the OCV was much lower (ca. 25 V) compared to SOFC due to 80% of steam in the fuel gas composition. Moreover, in SOEC, voltage fluctuations were observed, which were caused by instable vaporization of water in the steam generator. This is a well-known issue in SOEC operation. The voltage fluctuations increased with increasing current density. After 1,000 h of stack operation these voltage fluctuations could be minimized (see Figure 4) by an optimization of the steam generator operating parameters, e.g., the vaporization temperature of the steam generator and the water quality.

At low current densities the electrolysis voltage increased almost linearly with increasing current density. EIS spectra measured in this current regime have shown lower fuel electrode polarization and gas concentration resistances compared to SOFC operation. The stack temperature decreased with increasing current density (see Figure 3). This behavior is caused by the endothermic reaction of the water electrolysis (endothermic mode). After having passed a local temperature minimum at a current density of –250 mA cm^{-2}, the stack temperature increased. This resulted in a decrease of the electrolysis overvoltages and a flattening of the *J–V*-curve at higher current densities.

At –490 mA cm^{-2} the stack temperature reached 820 °C, which equals the temperature at OCV. At this operating point the stack voltage was almost 40 V, which corresponds to an average RU voltage of 1.32 V. This voltage is very close to the theoretical thermo-neutral voltage of 1.29 V, where the heat generated by the overvoltages equals the required entropic heat for the electrolysis. The measured value is higher compared to the theoretical one, because the stack has not fully reached thermal equilibrium during the increasing *J–V* measurement. For the decreasing *J–V*-curve (not shown in Figure 3) the situation is *vice versa* and the measured thermo-neutral voltage of 1.24 V was lower compared to the theoretical value. A further increase of the current density in Figure 3 led to a further increase of the stack temperature. In this case the energy supplied by the overvoltages exceeded the required thermal energy for the electrolysis and the electrolysis process switched to the exothermic mode.

In order to split 70% of the supplied steam, an electrolysis voltage of 40 V at a current density of ca. –520 mA cm^{-2} was required. This corresponded to a stack power of ca. –2.7 kW and a power density of approximately –700 mW cm^{-2}. At this operating point 14 SLPM of H_2 were produced at an electrical stack efficiency of ca. 94%. The highest electrical efficiency of 99% was achieved at 38 V (–375 mA cm^{-2}) and 50% steam conversion. At the highest current density of -650 mA cm^{-2} a steam conversion rate of 86%, 17.2 SLPM of produced H_2 and an electrical efficiency of ca. 93% were achieved. These initial SOEC performance data are very good in comparison to literature stack performance values [7, 10, 15–18, 24, 33]. Similar to SOFC operation, RU 1, 11, 21, and 30 on the bottom plate, on the intermediate and under the top stack plate showed slightly poorer SOEC performances compared to the other RUs due to higher contact resistances. However, in general the stack showed a very good SOEC performance in the beginning of the tests.

3.2 Long-Term Stability in SOEC Operation

Figure 4 shows the stack voltage and the stack temperature during 3,570 h of SOEC operation. The first 200 h were dedicated for initial characterization in SOFC and SOEC mode followed by 3,370 h of SOEC operation at 820 °C (at OCV) under constant current density of –520 mA cm^{-2}, which corresponds to 70% steam conversion. The spikes in Figure 4 represent the recordings of *J–V*-curves and EIS spectra. Moreover, the stack experienced 3 cooling down/heating up processes due to maintenance issues of the laboratory and the test station.

During 3,370 h of SOEC operation, the OCV of the stack remained almost constant, which can be attributed to the high quality and long-term stability of the glass sealing of the cells in the stack. In electrolysis operation at 70% SC voltage degradation rates of ca. +6.4 mV kh^{-1} per RU and +0.5% kh^{-1} were determined. These values are rather low compared to literature results, which report stack degradation rates between +0.6% kh^{-1} and +13.0% kh^{-1} [6, 7, 9–11, 14–18].

During SOEC operation, the stack temperature increased in total by 10 °C with a rate of 3.0 K kh^{-1}, which can be attributed to the increase of resistances (see Figure 9). The stack ASR increased by +370 mΩ cm^2 kh^{-1}, which corresponds to an average ASR degradation of ca.+12 mΩ cm^2 kh^{-1} for the RUs. The repeat units at the bottom of the stack (RUs 1–4) had higher

ORIGINAL RESEARCH PAPER

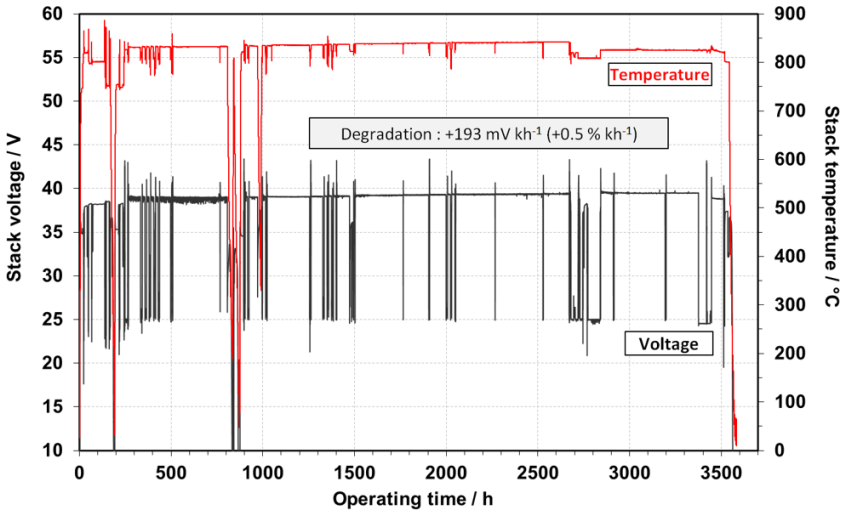

Fig. 4 Long-term behavior of the SOC stack during 3,570 h of SOEC operation at 820 °C, a current density of –520 mA cm^{-2} (70% SC) with fuel gas of 80% H_2O + 9% H_2 + 11% N_2 and air.

voltage degradation rates with values between +1.0% kh^{-1} and +1.4% kh^{-1}, whereas the degradation of the other RUs were in the range from +0.3% kh^{-1} to +0.7% kh^{-1}. EIS spectra have shown that this effect can mainly be attributed to different increases of the ohmic contact resistance of the RUs. This issue will be discussed in Section 3.6.

3.3 Long-Term Stability in Reversible SOFC/SOEC Operation

In Figure 5 the voltage and temperature of the SOC stack during 2,500 h of reversible SOFC/SOEC cycling operation is plotted. During this time, a total number of 92 SOEC cycles and 97 SOFC cycles were achieved. The interruptions between the cycles represent measurements of *J–V*-curves and EIS spectra as well as 2 cooling down/heating up processes for test station maintenance. Due to an increase of the stack temperature in SOEC mode at 5,170 h of operation, the electrical current density and fuel gas flow rate for the SOEC cycles had to be reduced (see Table 1) in order to remain below the maximum stack temperature of 860 °C.

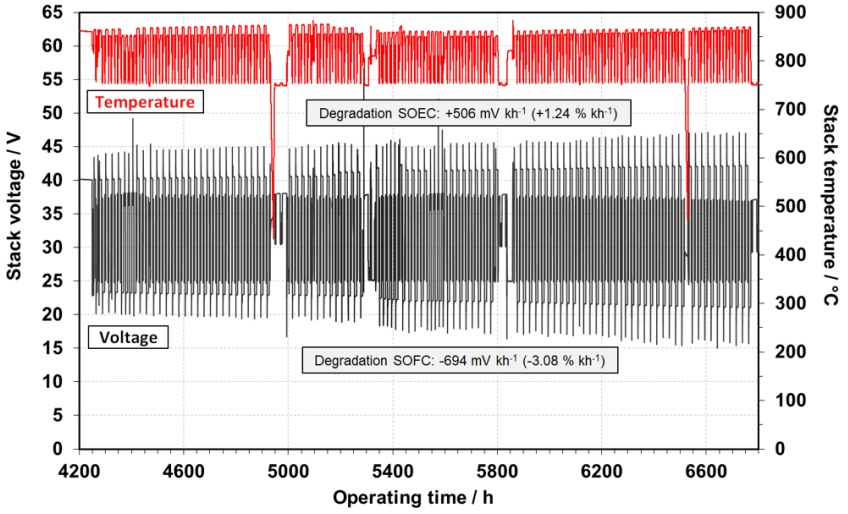

Fig. 5 Long-term behavior of the SOC stack during 2,500 h of reversible SOFC/SOEC operation (SOFC: 750 °C, 40% H_2 + 60% N_2, 70% FU / SOEC: 820 °C, 80% H_2O + 9% H_2 + 11% N_2, 70% SC).

The temperature between SOFC and SOEC mode under electrical current changed about 120 °C. During reversible operation, the stack temperature increased by ca. 7 K kh^{-1} in SOFC mode and 9 K kh^{-1} in SOEC mode. The OCVs of the RUs degraded by –1.2 mV kh^{-1} (–0.14% kh^{-1}) in SOEC mode and –17 mVkh^{-1} (–1.3% kh^{-1}) in SOFC mode. This issue will be discussed in more detail in Figure 6 in the next section. The voltage degradation in SOEC mode at 70% SC amounted to +17 mV kh^{-1} per RU or +1.2% kh^{-1}. This corresponds to a ASR increase of +39 mΩ cm^2 kh^{-1} per RU. In SOFC mode a voltage degradation of ca. –23 mV kh^{-1} per RU or -3.1% kh^{-1} was determined at 70% FU. The corresponding ASR increase of the RUs was +3.9 Ω cm^2 kh^{-1}. Even though the degradation in reversible operation was higher compared to SOEC peration, these reversible degradation values are much lower compared to stack results of other research groups [19, 20].

3.4 Comparison of Degradation in SOEC and Reversible SOFC/SOEC Operation

Figure 6 shows the comparison of the degradation (OCV, voltage and ASR) during stack operation in SOEC and reversible SOFC/SOEC operation. The values were extracted from the long-term measurements (Figures 4 and 5) and were normalized for the repeat units.

Figure 6 shows, that the OCV of the RUs measured under SOFC conditions degraded by –1.9 mV kh^{-1} in SOEC operation and by –17 mV kh^{-1} in reversible SOFC/SOEC operation. The corresponding OCV decreases, measured under SOEC conditions were much lower, which can be explained by a lower sensitivity of the OCV for a fuel gas composition with high steam content. The degradation of the OCVs of the individual RUs was quite inhomogeneous. This indicates that the gas tightness of the stack was much more affected by the reversible operation compared to the pure SOEC operation. In this context, temperature changes of 120 °C (see Figure 5) during reversible operation played an important role. Moreover, maximum temperature gradients between the middle and the bottom/top of the stack of about +30 °C in SOFC and –8 °C in SOEC were measured during cycling. It is very likely, that the resulting thermomechanical stresses have lowered the gas tightness of the

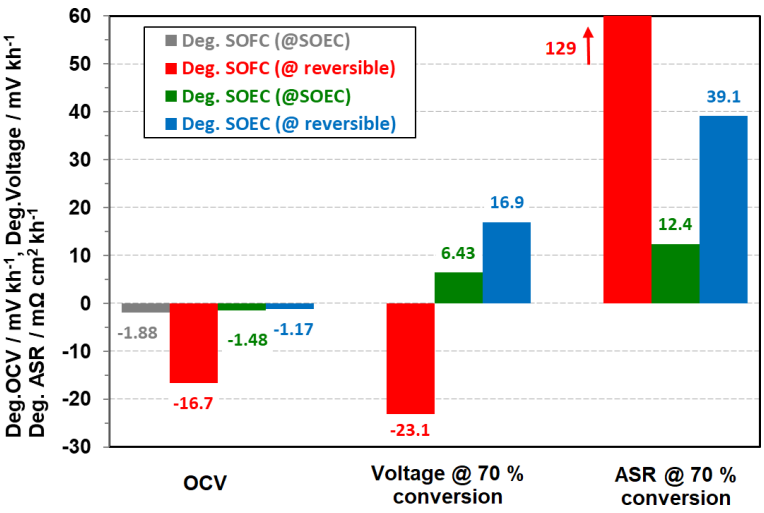

Fig. 6 Degradation of the RUs during 3,570 h of SOEC operation and during 2,500 h of reversible SOFC/SOEC operation.

glass sealing of the cells in the stack. It is very likely, that these thermomechanical stresses were quite inhomogeneous, which might explain the different OCV decrease values of the RUs.

Similar to the stack, all RUs showed higher degradation rates in reversible operation compared to SOEC operation. In comparison to the electrolysis voltage degradation of +6.4 mV kh^{-1} in pure SOEC operation, the degradation of the RUs in reversible operation mode rose to +17 mV kh^{-1} in SOEC and –23 mV kh^{-1} in SOFC, respectively. In this context, repeat units at the bottom of the stack (RU 1–RU 3) as well as the repeat unit on top of the intermediate plate (RU 11) had higher voltage degradation rates compared to the other RUs. This issue will be discussed below in Section 3.6.

The reason for these voltage degradations was the increase of the ASRs of the RUs. The lowest ASR increase of +12 mΩ cm^2 kh^{-1} was observed during pure SOEC operation. In contrast to that, the reversible operation has led to a high ASR increases of +130 mΩ cm^2 kh^{-1} in SOFC and +39 mΩ cm^2 kh^{-1} in SOEC mode. The reasons for these different degradation rates are discussed below. The observed higher stack degradation in reversible operation is in good agreement with [19], where thermomechanical stress induced crack formation and delamination effects are reported. In general, the thermomechanical stresses during reversible operation strongly depend on the stack or the cell design. Therefore, the degradation results of reversibly operated single cells, as reported in [34–36], might differ from the stack degradation results of the present paper. For single cells, degradation values in reversible SOFC/SOEC and pure SOEC operation are reported to be similarly high [34, 35] or even lower in reversible operation [36].

3.5 EIS Spectra in SOEC and SOFC Mode During Long-Term Operations

In order to qualify but not to quantify the differences between pure SOEC and reversible SOFC/SOEC operations, EIS spectra of selected RUs were measured regularly during the long-term tests. Please note, that the spectra were measured at a very low electrical current density of ±15.6 mA cm^{-2}, in order to exclude electrical current induced temperature effects. Therefore, the corresponding impedance values refer to the low current density region (see Figure 3) and are much higher compared to the above calculated ASR values from the long-term operations under electrical current load. Figure 7 shows the EIS spectra of repeat unit RU 14 in electrolysis mode at different operating times during SOEC and reversible SOFC/SOEC operation. The EIS spectra were measured at a stack temperature of 820 °C with a gas composition of 80% H_2O + 9% H_2 + 11% N_2 and air.

In the EIS spectra, plotted as a Cole-Cole diagram in Figure 7, the ohmic resistance of the repeat unit is represented by the high frequency impedance above 1 kHz, whereas the overall impedance is measured at low frequencies below 25 mHz. Altogether three frequency dependent processes can be identified as depressed half-circles. These processes are the steam reduction to H_2 at the fuel electrode in the high frequency range (ca. 1 kHz–100 Hz), the oxidation of O^{2-}-ions to O_2 at the air electrode in the middle frequency range (ca. 100 Hz-5 Hz) and the gas concentration/diffusion process at the fuel electrode at low frequencies (ca. 5 Hz-25 mHz). Because of the high flow rate of air, gas concentration/transport impedances at the air electrode are negligible. These impedance results are in good agreement with the results of other research groups [8, 10, 13, 14, 24, 35, 37]. In this context it has to be mentioned, that the EIS spectra strongly depend on materials and geometries of the cells/stacks as well as on the operating conditions, which can complicate the reliable interpretation of the EIS data [38].

With proceeding operating time all impedance spectra showed a similar curve progression, while the overall impe-

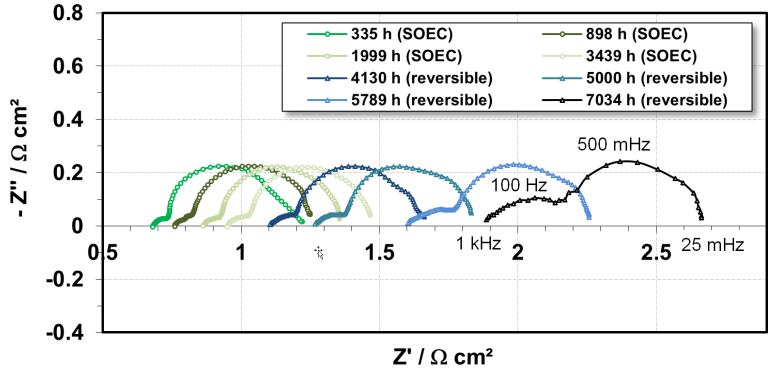

Fig. 7 Impedance spectra of RU 14 measured at SOEC conditions at 820 °C near OCV (–15.6 mA cm^{-2}) with 80% H_2O + 9% H_2 + 11% N_2 and air at different operating times.

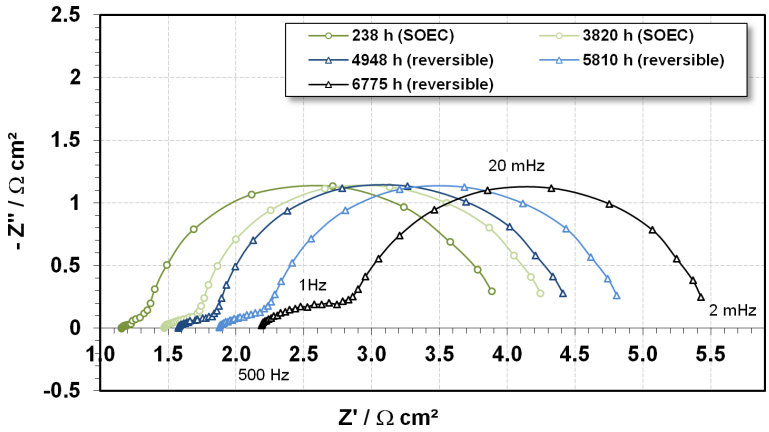

Fig. 8 Impedance spectra of RU 14 measured at SOFC conditions at 750 °C near OCV (15.6 mA cm^{-2}) with 40% H_2 + 60% N_2 and air at different operating times.

dance significantly increased from approximately 1.2 Ω cm^2 after 335 h to 2.7 Ω cm^2 after 7,034 h of operation. While the polarization resistance represented by the first half circle at low frequencies showed a relatively low increase over time, the ohmic resistance increased significantly from 0.7 Ω cm^2 to 1.9 Ω cm^2.

Figure 8 shows the EIS spectra of RU 14 in fuel cell mode at different operating times during SOEC and reversible SOFC/SOEC operation. The EIS spectra were measured in SOFC mode at a stack temperature of 750 °C, an applied current density of 15.6 mA cm^{-2} and with a gas composition of 40% H_2 + 60% N_2 and air. The EIS spectra in SOFC mode show higher ohmic resistances and lower frequency ranges of the corresponding electrochemical processes compared to the spectra in SOEC mode. This can be explained by a lower stack temperature in SOFC (750 °C) compared to SOEC mode (820 °C). Moreover, due to dry fuel gas in SOFC, the gas concentration impedance was significantly higher compared to the spectra in SOEC (Figure 7). The gas concentration impedance is caused by diffusive and convective gas phase transport processes in the fuel electrode support substrate and the fuel electrode itself [39, 40]. In SOFC this impedance strongly depends on the fuel gas composition and has a minimum at 50% steam in the fuel gas [41]. During long-term operation, all EIS spectra degraded in a similar way, while the overall impedance significantly increased from approximately 3.9 Ω cm^2 after 238 h to 5.5 Ω cm^2 after 6,775 h of operation. The gas concentration impedance remained almost constant, whereas the polarization impedance and ohmic resistance increased significantly. The ohmic resistance increased from approximately 1.2 Ω cm^2 to 2.2 Ω cm^2. The degradation of the resistances is discussed more detailed in the following Section 3.6.

3.6 Resistances in SOFC and SOEC Mode During Long-Term Operations

In Figure 9 the time-dependent behavior of the ohmic resistance, the electrode polarization resistance and the gas concentration resistance of RU 14 in SOEC mode at different operating times during SOEC operation and reversible SOFC/SOEC operation is plotted. The gas concentration resistance remained relatively stable during SOEC (–3.5 mΩ cm^2 kh^{-1}) and reversible operation (+18 mΩ cm^2 kh^{-1}). The electrode polarization resistance also remained relatively constant (+8.7 mΩ cm^2 kh^{-1}) during SOEC operation but increased significantly with a rate of +59 mΩ cm^2 kh^{-1} in reversible operation. In this context, it cannot be excluded that part of the higher degradation rate in reversible mode is simply due to stack age. It is very likely, that impurities, e.g., silicon and sulfur, in the steam (Si ca. 40 µg L^{-1}, S ca. 20 µg L^{-1}) fed to the stack and/or from the glass sealings were accumulated during the operation in the fuel gas electrodes. These impurities are known to increase the fuel electrode polarization resistance [4, 42–44]. Additionally, other well-known degradation mechanisms, e.g., agglomeration and/or depletion of Ni in the fuel electrode [4, 11, 12, 44, 45] and ion demixing and Cr-poisoning in the air electrode [4, 12, 44, 46] are likely to contribute to the observed electrode degradation. Compared to RU 14, the RUs at the bottom of the stack (RU 1–RU 4) showed higher increases .of the electrode polarization impedances. After operation some Cr-oxide formation was observed preferentially at the air inlet at the bottom of the stack (see also stack before operation in Figure 2). In this context, Cr-evaporation from the air tubes and the gas distribution plate and a possible air flow distribution gradient over the height of the stack may play an important role. This might have caused higher Cr-poisoning of the air electrodes of the

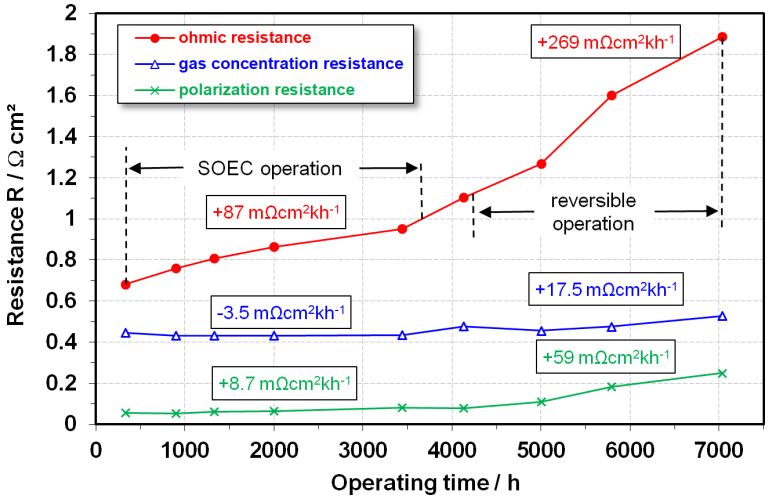

Fig. 9 Resistances of RU 14 measured at SOEC conditions at 820 °C near OCV (–15.6 mA cm^{-2}) with 80% H_2O +9% H_2 + 11% N_2 and air at different operating times. The given degradation rates serve as qualitative comparison and have limited quantitative meaning.

bottom cells, resulting in the observed slightly higher degradation rates. The ohmic resistance showed the highest increase among the resistances with proceeding operating time. The ohmic resistance degradation of +87 $m\Omega\,cm^2\,kh^{-1}$ in SOEC operation rose to 270 $m\Omega\,cm^2\,kh^{-1}$ in reversible operation. Hence, the main degradation in SOEC can be attributed to the increase of the ohmic resistance in both operations, but with a much higher value in reversible SOFC/SOEC operation. Concerning the ohmic degradation mechanisms, the formation of voids [4, 44, 46] and of Sr-zirconate [4, 12, 44, 45] at the interface between electrolyte and GDC barrier layer and delamination of the air electrode [11, 20, 45] are the most probable ones. The observed higher degradation of the RUs at the intermediate plates, especially RU 11, may be caused by electrical ohmic contact degradation.

Figure 10 shows the time-dependent behavior of the polarization resistance, gas concentration resistance as well as ohmic resistance in SOFC mode during SOEC and reversible SOFC/SOEC operation. The gas concentration resistance remained relatively stable with rates of +5.6 $m\Omega\,cm^2\,kh^{-1}$ during SOEC operation and +10 $m\Omega\,cm^2\,kh^{-1}$during reversible SOFC/SOEC operation. This can be explained by the almost constant OCV of this RU. Another effect may be the above mentioned coarsening of the porous structure of the fuel electrode, which may increase the diffusion length for the fuel gas, thus increasing the gas concentration resistance [41]. The degradation rate of the ohmic resistance increased from +82 $m\Omega\,cm^2\,kh^{-1}$ in SOEC operation to ca. +250 $m\Omega\,cm^2\,kh^{-1}$ in reversible operation. Similar to the values under SOEC conditions, the increase in ohmic resistance was the main degradation effect and highest in reversible SOFC/SOEC operation. The rate of change of the polarization resistance rose from +21 $m\Omega\,cm^2\,kh^{-1}$ in SOFC operation to ca. +120 $m\Omega\,cm^2\,kh^{-1}$ in reversible operation.

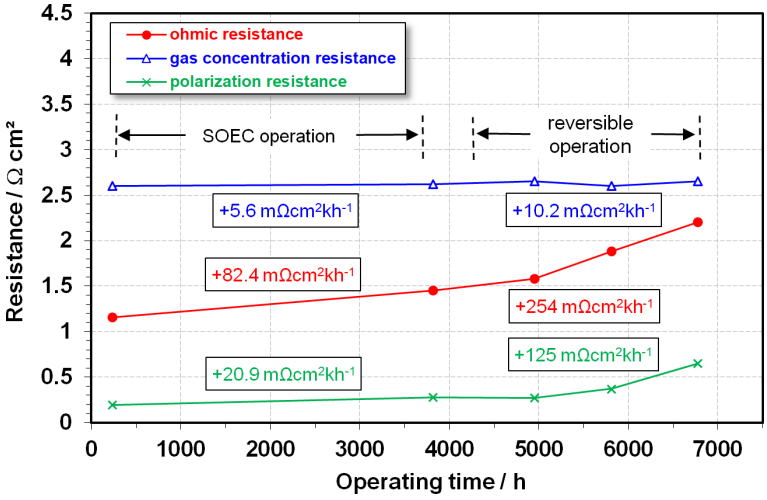

Fig. 10 Resistances of RU 14 measured at SOFC conditions near OCV (15.6 mA cm^{-2}) with 40% H_2 + 60% N_2 and air at different operating times. The given degradation rates serve as qualitative comparison and have limited quantitative meaning.

4 Conclusions

A 30-cell stack with ESCs was operated for 3,370 h in SOEC and for 2,500 h in reversible SOFC/SOEC cycling mode at 70% steam conversion and 70% fuel utilization, respectively. In the beginning of the test, the stack showed a high gas tightness and good initial behavior in SOEC and SOFC operation. In SOFC operation the stack reached an electrical efficiency of 44.1% at a fuel utilization of 70%. In SOEC operation an electrical efficiency of 94.2% at a steam conversion of 70% was achieved. These initial performance values are high compared to literature values. During 3,370 h of SOEC operation at 820 °C and 70% SC, the stack remained gas-tight and the electrolysis voltage increased by +0.5% kh^{-1} (i.e., +12 $m\Omega\,cm^2\,kh^{-1}$ per RU), which is low compared to the degradation of other stacks found in literature. During 2,500 h of reversible SOFC/SOEC cycling operation, an OCV decrease was observed, which can be explained by degradation of the glass sealing due to thermomechanical stresses during reversible cycling. However, sufficient gas tightness of the stack was ensured throughout the 7,500 h of operation. During reversible cycling, an electrolysis voltage degradation rate of +1.2% kh^{-1} (i.e., +39 $m\Omega\,cm^2\,kh^{-1}$ per RU) was measured, which is more than twice as high compared to the non-cycled SOEC operation. Moreover, the fuel cell voltage during reversible SOFC/SOEC cycling operation decreased with a high degradation rate of –3.1%/1,000 h. In this context, it cannot be excluded that part of the higher degradation rate in reversible mode is simply due to stack age. EIS spectra have shown that the increase of the ohmic resistance contributed mostly to the degradation rates. Also an increase of the electrode polarization resistance was observed. During reversible SOFC/SOEC cycling, the electrode polarization resistance and ohmic resistance degraded much faster compared to non-cycled SOEC operation. In contrast to that, the gas concentration resistance remained almost constant during SOEC and reversible SOFC/SOEC operation. Optimized operating conditions for reversible cycling in order to minimize thermomechanical stresses and the increase in purity of the supplied process media (gases and water) are measures in order to lower the stack degradation. Moreover, post-mortem analysis of the stack after operation will help to identify the material and structural degradation mechanisms in the stack components. These activities will help to understand the degradation of SOC stacks and to further improve their lifetime for power-to-gas-applications.

Acknowledgements

The German Federal Ministry of Transport and Digital Infrastructure (BMVI) is gratefully acknowledged for the funding of the RSOC project under the grant agreement number 03B10901B2. Open access funding enabled and organized by Projekt DEAL.

List of Symbols

$f_{i,\,in}$	Flow rate of component *i* of the gas into the fuel gas electrode / slpm, L min^{-1}
$f_{i,\,out}$	Flow rate of component *i* of the gas out of the fuel gas electrode / slpm, L min^{-1}
FU	Fuel utilization in SOFC mode / %
ΔrH	Enthalpy of reaction / kJ mol^{-1}
LHV_i	Lower heating value of fuel gas component *i* / J mol^{-1}
N	Number of repeating units in the stack / –
$\eta_{el,LHV}$	Electrical efficiency based on LHV of fuels / %
η_0	Irreversible voltage losse / V
P_{el}	Electrical power of the cell/stack / W
p_i	Partial pressure of component *i* in the gas of the fuel gas electrode / mbar, kPa
R	Resistance / Ω, Ω cm^2
U_{gas}	Gas utilization at the fuel electrode (fuel utilization in SOFC mode, steam conversion in SOEC mode) %
SC	Steam conversion in SOEC mode / %
V^0_{rev}	Theoretical thermodynamic reversible voltage for partial pressure 1 / V
V_{tn}	Thermoneutral voltage / V
V_{mol}	Molar volume of gas / L mol^{-1}
z	Number of exchanged electrons / –
Z	Impedance / Ω, Ω cm^2
Z′	Real part of impedance / Ω, Ω cm^2
Z′′	Imaginary part of impedance / Ω, Ω cm^2

References

[1] W. Doenitz, R. Schmidberger, E. Steinheil, R. Streicher, *Int. J. Hydrog. Energy* **1980**, *5*, 55.

[2] S. Dutta, *Int. J. Hydrog. Energy* **1990**, *15*, 379.

[3] T. L. Skafte, J. Hjelm, P. Blennow, C. R. Graves, *Proc. 12th Europ. SOFC & SOE Forum* **2016**, *06*, 8–26.

[4] P. Mocoteguy, A. Brisse, *Int. J. Hydrog. Energy* **2013**, *38*, 15887.

[5] J. R. Mawdsley, J. D. Carter, A. J. Kropf, B. Yildiz, V. A. Maroni, *Int. J. Hydrog. Energy* **2009**, *34*, 4198.

[6] J. Schefold, A. Brisse, M. Zahid, *ECS Trans.* **2010**, *28*, 357.

[7] J. Schefold, A. Brisse, M. Zahid, J. P. Ouweltjes, J. U. Nielsen, *ECS Trans.* **2011**, *35*, 2915.

[8] S. D. Ebbesen, J. Høgh, K. A. Nielsen, J. U. Nielsen, M. Mogensen, *Int. J. Hydrog. Energy* **2011**, *36*, 7363.

[9] A. Brisse, J. Schefold, *Energy Procedia* **2012**, *29*, 53.

[10] Q. Fang, L. Blum, N. H. Menzler, *J. Electrochem. Soc.* **2015**, *162*, F907.

[11] Q. Fang, C. E. Frey, N. H. Menzler, L. Blum, *J. Electrochem. Soc.* **2018**, *162*, F38.

[12] C. E. Frey, Q. Fang, D. Sebold, L. Blum, N. H. Menzler, *J. Electrochem. Soc.* **2018**, *165*, F357.

[13] Y. Yan, Q. Fang, L. Blum, W. Lehnert, *Electrochim. Acta* **2017**, *258*, 1254.

[14] Q. Fu, J. Schefold, A. Brisse, J. U. Nielsen, *Fuel Cells* **2014**, *14*, 395.

[15] M. Petitjean, M. Reytier, A. Chatroux, L. Bruguière, A. Mansuy, H. Sassoulas, S. Di Iorio, B. Morel, J. Mougin, *ECS Trans.* **2011**, *35*, 2905.

[16] Y. Zheng, Q. Li, T. Chen, W. Wu, C. Xu, W. G. Wang, *Int. J. Hydrog. Energy* **2015**, *40*, 2460.

[17] X. Zhang, J. E. O'Brien, R. C. O'Brien, J. J. Hartvigsen, G. Tao, G. K. Housley, *Int. J. Hydrog. Energy* **2013**, *38*, 20.

[18] M. Riedel, M. P. Heddrich, K. A. Friedrich, *Int. J. Hydrog. Energy* **2019**, *44*, 4570.

[19] J. Hong, H.-J. Kim, S.-Y. Park, J.-H. Lee, S.-B. Park, J.-H. Lee, B.-K. Kim, H.-J. Je, J. Y. Kim, K. J. Yoon, *Int. J. Hydrog. Energy* **2014**, *39*, 20819.

[20] N. Q. Minh, *ECS Trans.* **2011**, *35*, 2897.

[21] V. N. Nguyen, Q. Fang, U. Packbier, L. Blum, *Int. J. Hydrog. Energy* **2013**, *38*, 4281.

[22] O. Posdziech, K. Schwarze, J. Brabandt, *Int. J. Hydrog. Energy* **2019**, *44*, 19089.

[23] T. Strohbach, F. Mittmann, C. Walter, D. Schimanke, C. Geipel, *ECS Trans.* **2015**, *68*, 125.

[24] M. Preininger, V. Subotic, B. Stoeckl, R. Schauperl, D. Reichholf, S. Megel, M. Kusnezoff, C. Hochenauer, *Int. J. Hydrog. Energy* **2018**, *43*, 12398.

[25] M. Lang, S. Raab, M. S. Lemcke, C. Bohn, M. Pysik, *ECS Trans.* **2019**, *91*, 2713.

[26] M. Lang, C. Bohn, K. Couturier, X. Sun, S. J. McPhail, T. Malkow, A. Pilenga, Q. Fu, Q. Liu, *J. Electrochem. Soc.* **2019**, *166*, F1180.

[27] International Electrotechnical Commission (IEC), *Technical specification document 62282-1 TS Ed.3: Fuel cell technologies / Part 1: Terminology*, can be found under https://webstore.iec.ch/publication/6751, **2013**.

[28] International Electrotechnical Commission (IEC), *Technical specification document 62282-7-2 TS Ed.1: Fuel cell technologies / Part 7-2: Single cell/stack performance test methods for solid oxide fuel cells (SOFC)*, can be found under https://webstore.iec.ch/publication/6766, **2014**.

[29] D. R. Lide, *CRC Handbook of Chemistry and Physics*, 78th Ed., CRC Press, Boca Raton, Fl, USA,, **1997**, pp. 5–77.

[30] ThyssenKrupp VDM GMBH, *Crofer 22 APU Material Data Sheet No. 4046*, can be found under http://www.vdm-metals.com/fileadmin/user_upload/Downloads/Data_Sheets/Data_Sheet_VDM_Crofer_22_APU.pdf, **2010**.

[31] C. A. Schiller, *Electrochem. Applications*, Zahner-elektrik GmbH & Co. KG, **1997**, *1/97*, 10.

[32] M. Lang, C. Bohn, M. Henke, G. Schiller, C. Willich, F. Hauler, *J. Electrochem. Soc.* **2017**, *164*, F1460.

[33] M. Preininger, B. Stoeckl, V. Subotić, R. Schauperl, C. Hochenauer, *ECS Trans.* **2019**, *91*, 2589.

[34] F. Petipas, Q. Fu, A. Brisse , C. Bouallou, *Int. J. Hydrog. Energy* **2013**, *38*, 2957.

[35] X. Sun, B. R. Sudireddy, X. Tong, M. Chen, K. Brodersen, A. Hauch, *ECS Trans.* **2019**, *91*, 2631.

[36] C. Graves, S. D. Ebbesen, S. H. Jensen, S. B. Simonsen, M. B. Mogensen, *Nature Materials* **2015**, *14*, 239.
[37] E.-C. Shin, P.-A. Ahn, H.-H. Seo, J.-M. Jo, S.-D. Kim, S.-K. Woo, J. H. Yu, J. Mizusaki, J.-S. Lee, *Solid State Ionics* **2013**, *232*, 80.
[38] A. Nechache, M. Cassir, A. Ringuedé, *J. Power Sources* **2014**, *258*, 164.
[39] S. Primdahl, M. Mogensen, *J. Electrochem. Soc.* **1998**, *145*, 2431.
[40] W. G. Bessler, *J. Electrochem. Soc.* **2006**, *153*, 1492.
[41] J. Geyer, H. Kohlmüller, H. Landes, R. Stubner, *ECS Proc. 5th International Symposium on Solid Oxide Fuel Cells (SOFC-V)* **1997**, 1997-40, 585.
[42] S. D. Ebbensen, C. Graves, A. Hauch, S. H. Jensen, M. Mogensen, *J. Electrochem. Soc.* **2010**, *157*, 1419.
[43] A. Hauch, S. D. Ebbensen, S. H. Jensen, M. Mogensen, *J. Electrochem. Soc.* **2008**, *155*, 1184.
[44] K. Chen, S. P. Jiang, *J. Electrochem. Soc.* **2016**, *163*, 3070.
[45] N. H. Menzler, D. Sebold, S. Zischke, *ECS Trans.* **2019**, *91*, 719.
[46] F. Tietz, D. Sebold, A. Brisse, J. Schefold, *J. Power Sources* **2013**, *223*, 129.

